Journal of Manufacturing Processes 22 (2016) 34–38

Contents lists available at ScienceDirect

Journal of Manufacturing Processes

journal homepage: www.elsevier.com/locate/manpro

Spraying of Fe-based amorphous coating with high corrosion resistance by HVAF

Gang Wang*, Zhongjia Huang, Ping Xiao, Xiebing Zhu

Remanufacturing Surface Engineering Technology Research Center, Anhui Polytechnic University, Wuhu 241000, PR China

ARTICLE INFO

Article history:
Received 7 May 2015
Received in revised form 28 January 2016
Accepted 28 January 2016

Keywords:
Amorphous alloy
Coating
HVAF
Corrosion resistance

ABSTRACT

Fe-based amorphous coating with composition of $Fe_{42.87}Cr_{15.98}Mo_{16.33}C_{15.94}B_{8.88}$ has been deposited on a mild steel substrate by high velocity air fuel thermal spraying. The microstructure and corrosion properties of the Fe-based alloy coating were studied in detail. It was found that the obtained Fe-based coating showed fully amorphous state with about 100 μm in thickness. Also, the obtained coating exhibited very dense structure with a porosity of 1.5%. Polarization tests demonstrated that the coating exhibited better corrosion resistance than stainless steel in NaOH solution and simulated seawater. The reasons of superior corrosion have been discussed from the alloy elements and the homogeneous structure of Fe-based amorphous coating.

1. Introduction

Due to the lack of grain boundaries and dislocations, metallic glasses have gained an interest of their well combinations high strength, high elastic limit, excellent wear resistance, and superior corrosion resistance [1]. So far, numerous metallic glasses with high glass forming ability have been explored in Ti- [2], Zr- [3], Fe- [4], and Cu-based alloy systems [5]. However, the limited glass formation ability has significantly hindered the range of engineering applications. In order to widen their industrial application fields, the route of spraying as coating has been recognized as an efficient way to overcome the drawback [6]. In the past years, several coating technologies have been used to fabricate amorphous coatings, such as plasma spraying [7], arc spraying [8,9], laser surface process [10,11], high velocity oxygen fuel spraying (HVOF) [12,13], high velocity air fuel spraying (HVAF) [14,15], and so on. Compared with the methods mentioned above, HVOF thermal spraying is one of the most widely used process for depositing coatings such as metals, cermets, ceramics, and metallic glasses, which seems more feasible due to its high cooling rate of 10^7–10^{10} K/s[16]. However, in comparison with the HVOF process, HVAF system which combusts a mixture of compressed air and fuel gas in the combustion chamber has a lower spraying temperature (1600 K) than HVOF (1900 K) process. So, the chemical uniformity by controlled oxidation in the coating by HVAF can be improved [17]. Moreover, the high particle velocity, typically over 700 m/s, of the HVAF process has been reported to provide lower porosity in the coating and well adhesion strength than HVOF. Furthermore, the use of air instead of oxygen for combustion by HVAF is expected to lower the cost of the spraying and promote its competitiveness over other processes [18]. Up to now, some attempts have been made on preparation of amorphous alloy coatings by means of HVAF process. Liu et al. have reported that Fe-based amorphous coatings were prepared by HVAF and HVOF processes on a mild steel substrate. Corrosion resistance in 3.5 wt % NaCl solution of the coatings prepared by the two processes was comparatively studied. The results demonstrate that HVAF with less cost can be a promising spray process to fabricate the Fe-based amorphous coating for industrial applications [14]. Ye et al. have carefully researched the influence of spraying parameters on coating by tuning the spraying gun length, spraying distance, and powder feed rate. Results indicate that spraying gun length is the key factor in forming perfect amorphous coating [19]. In previous studies, most of the coating prepared by HVAF has been studied, but the systematic studies on corrosion behavior is still lacking.

Among the metallic glasses systems being researched, Fe-based amorphous metallic glasses are considered to be extremely viable candidates as surface protective coatings owning to their high crystallization temperature, superior corrosion, good magnetic properties, and relatively low material cost. In this paper, a $Fe_{42.87}Cr_{15.98}Mo_{16.33}C_{15.94}B_{8.88}$ (at %) with high glass formation ability was selected to prepare amorphous alloy coating by HVAF

* Correspondence to: School of Mechanical and Automotive Engineering, Anhui Polytechnic University, Wuhu 241000, PR China. Tel.: +86 553 2871253; fax: +86 553 2871253.
E-mail addresses: gangwang@ahpu.edu.cn, wg10310918@163.com (G. Wang).

http://dx.doi.org/10.1016/j.jmapro.2016.01.009
1526-6125/

spraying. The microstructure and the morphology of the cross-section of the as-sprayed metallic glass coatings were examined. The corrosion behavior of the Fe-based metallic glass coating was assessed by comparing with different solution.

2. Experimental

A mixture of pure elements of Fe, Cr, Mo, C, and B with 99.9 wt % purity was induction melted under high purity argon atmosphere and then atomized. The chemical composition of atomized powder is $Fe_{42.87}Cr_{15.98}Mo_{16.33}C_{15.94}B_{8.88}$ (at %). The particle size distribution was examined by using a laser-assisted particle size analyzer (MS-2000). The mild steel (0.45 wt % C) was used as substrates with a dimension of $10 \times 10 \times 10\,mm^3$. All substrates were sand blasted followed by washing with acetone and methanol to clean the surface. The main spraying parameters are air pressure 0.62 MPa, fuel pressure 0.55 MPa, spraying distance 250 mm, and powder delivery rate 5 rpm. The percentage of porosity of the amorphous coatings was evaluated by SEM micrograph analysis using an Image Pro Plus software. Scanning electron microscopy (SEM), and X-ray diffraction (XRD) were used for the microstructure characterization and phase analysis of the gas-atomized powders and as-sprayed Fe-based alloy coatings. The corrosion behavior of the samples was evaluated by electrochemical measurement with a three-electrode cell using a platinum counter electrode and a saturated calomel reference electrode. The working electrode was exposed to an area of $1\,cm^2$. Electrolytes used were NaOH alkali solutions (0.5 mol/L, 1 mol/L, 2 mol/L), and 3.5% NaCl (mass %) aqueous solution which simulated seawater. Potentiodynamic polarization curves were measured with a potential sweep rate of 0.01 mV/s from −1 V to 1.5 V in all solutions open to air at 298 K after immersing the specimens with half-hour, when the open-circuit potentials became almost steady. For comparison, cast 304 stainless steel plates were also selected to perform the electrochemical measurements in the same way.

3. Results and discussion

Fig. 1(a) presents the SEM images of the Fe–Cr–Mo–C–B alloy powders. It can be seen that the majority of the particles produced by gas atomization in an argon atmosphere are spherical or near-spherical in shape. Some large powders have small satellites with a size of 10–15 μm, as shown the inset of Fig. 1a. During gas atomization process, some smaller particles in the powder experienced a higher solidification rate can easily adhere to the molten surfaces of larger particles, resulting in the formation of such attached particle morphology. Most of them exhibit smooth surface as the meaning of good fluidity [20]. Fig. 1(b) shows the size distribution of Fe-based alloy powders. It can be seen that the Fe-based alloy powders exhibit a lognormal size distribution. The particle size ranges from 20 to 50 μm, and the average particle diameter is 35 μm.

Fig. 2(a) shows the typical region from cross-sections of the coatings which reveal its dense layered structure, although, some pores exist as very dark regions can be seen. In general, the big pores located between flattened droplets are mainly caused by the loose packed layer structure of gas porosity phenomenon, while the small pores with the flattened particles originate from the shrinkage porosity. In despite of the presence of these defects, the coatings express a low porosity below 1.5% which is typical of AC-HVAF thermal sprayed deposits. During thermal spraying,

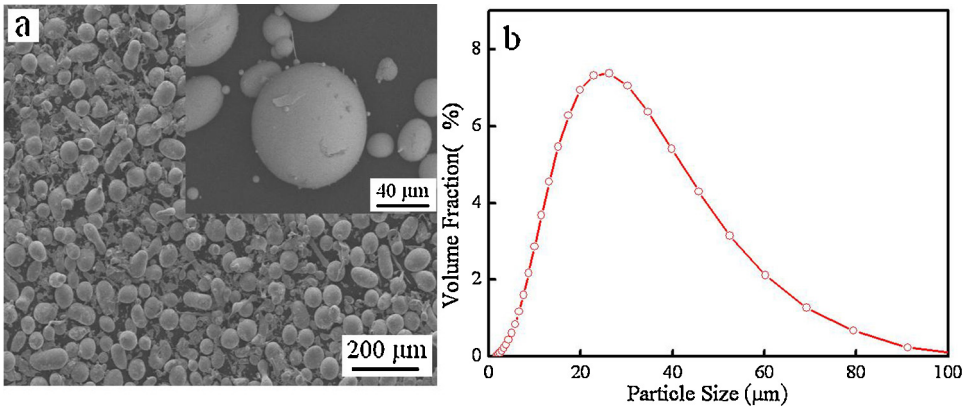

Fig. 1. (a) SEM images and (b) particle size distribution of Fe-based alloy powders.

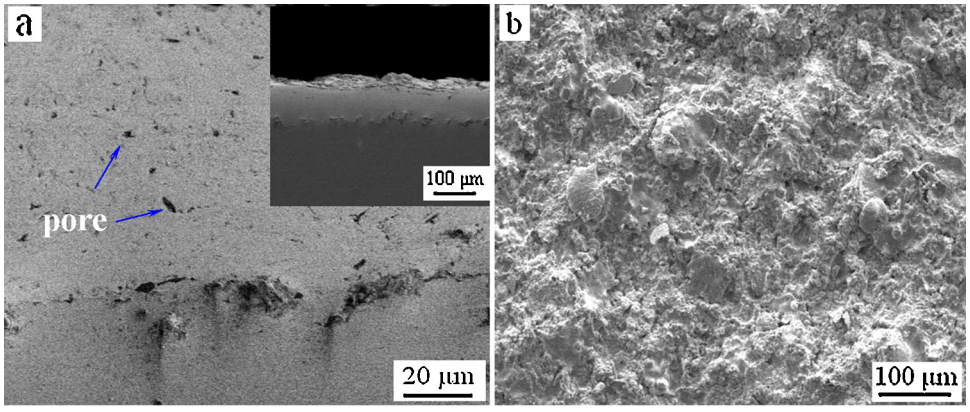

Fig. 2. (a) SEM image of cross-section and (b) planar view of Fe-based alloy coating.

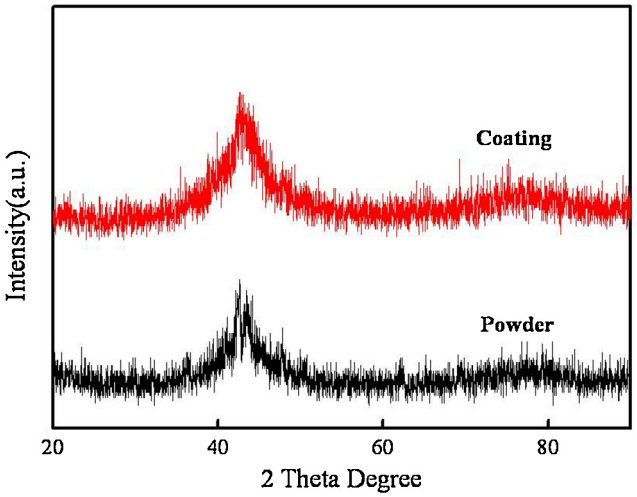

Fig. 3. XRD patterns of atomized powders and the as-deposited coating.

the deposition of successive molten droplets release latent heat in solidification, and localized reheating could occur, resulting in thermal softening by increasing the temperature of the particles to the values near the glass transition temperature of the amorphous alloy. This favors plastic deformation and mechanical interlocking of splats, cleans the surfaces of the particles and promotes metallurgical bonding at the particle/particle surface. Therefore, the coating obtained exhibits a relatively low porosity. The thickness of coating is about 100 μm, showing by the inset of Fig. 2(a). Fig. 2(b) shows the surface morphology of the coating. Individual particle exhibits well-flattened splat and near disk-sharp splat morphology with little splashing, indicating that the alloy system has excellent wetting behavior.

The XRD patterns of the atomized powders and as-deposited coating are shown in Fig. 3. It is notable that a single broad halo peak appearing in the samples indicates the high amorphous phase content, which is primarily attributed to the high glass formation ability of $Fe_{42.87}Cr_{15.98}Mo_{16.33}C_{15.94}B_{8.88}$ metallic alloy and high impact speed (>700 m/s) and cooling rate (>10^7 K/s) of AC-HVAF thermal spraying process. For the present alloy, the critical size for glass formation is 2.7 mm in diameter. Based on the relationship between critical size and cooling rate, the cooling rate for the glassy rod can be calculated to be about 550 K/s[21,22]. Such cooling rate is much lower than the cooling rate for powders during thermal spraying process which facilitate the formation of glassy phase. Based on the above analysis, Fe-based alloy coating obtained exhibits glassy structure in the present work.

Fig. 4 shows the potentiodynamic polarization curves of the as-deposited coatings with different solutions. It can be seen that all of the curves exhibit similar polarization behavior and are spontaneously passivated with low passive current density and wide passive region. This phenomenon suggests that the coatings have a prominent ability to resist localized corrosion in the NaOH solution, as shown in Fig. 4(a). At the beginning of the corrosion, the passivation films can rapidly be formed due to the existence of the Cr element in alloy system. Also, with the increasing solution concentration, it can be seen that the corrosion potential E_{corr} reduces, while the corrosion current density I_{corr} and the passivation current density I_{pass} increases. These indicate that the corrosion resistance of coatings decline in different NaOH solution. E_{corr}, I_{corr}, and I_{pass} obtained from the polarization curves are listed in Table 1. As seen, the Fe-based coating exhibits a lower corrosion current density (3.162×10^{-5} A/cm^2, 7.586×10^{-5} A/cm^2 and 1.502×10^{-4} A/cm^2) than 304 stainless steel, i.e., 2.884×10^{-4} A/cm^2, and higher corrosion potential (−0.306 V, −0.373 V, and −0.524 V) than stainless

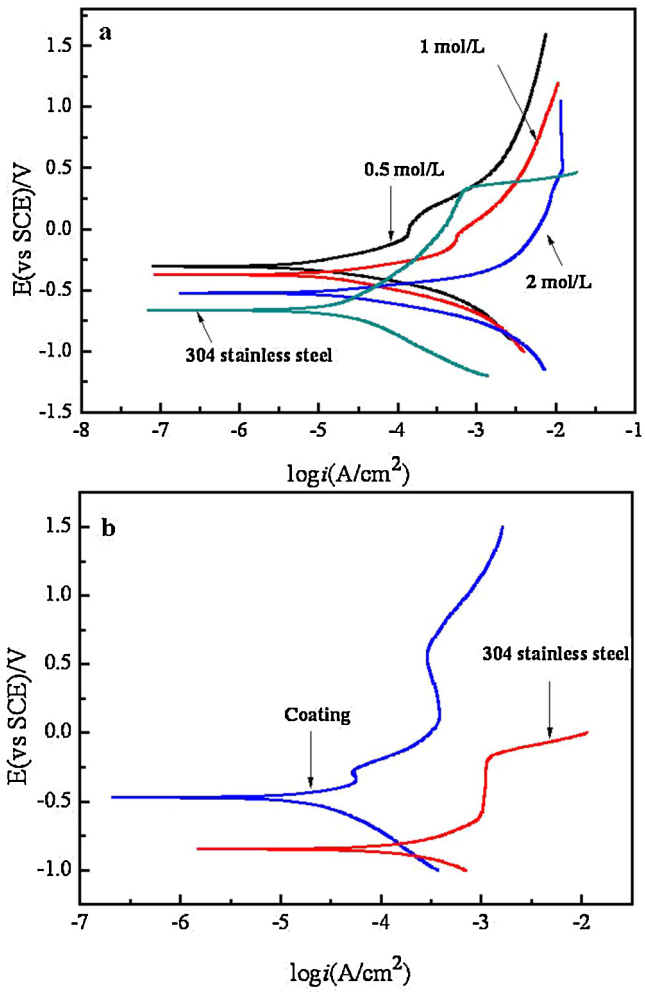

Fig. 4. The potentiodynamic polarization curves of the as-deposited coatings in different solution: (a) NaOH solution, and (b) 3.5% NaCl solution.

Table 1
Corrosion data determined from the polarization curves.

Alloys	E_{corr}(V)	I_{corr}(A/cm^2)	I_{pass}(A/cm^2)
Coating			
0.5 mol/L	−0.306	3.162×10^{-5}	7.499×10^{-3}
1 mol/L	−0.373	7.586×10^{-5}	1.082×10^{-2}
2 mol/L	−0.524	1.502×10^{-4}	1.148×10^{-2}
NaCl	−0.472	5.623×10^{-6}	3.715×10^{-4}
Stainless steel (2 mol/L)	−0.665	2.884×10^{-4}	5.129×10^{-2}
Stainless steel (NaCl)	−0.846	3.162×10^{-4}	9.661×10^{-4}

steel, i.e., −0.665 V, indicating that passive films formed in the amorphous coating are more protective. Since the difficulty of corrosion is influenced by the corrosion potential, the corrosion rate is determined by the corrosion current density. The higher the corrosion potential and the lower the corrosion current density, the more obvious is the corrosion resistance [16]. Moreover, it can be seen from Fig. 4 and Table 1 that the coating exhibits spontaneous passivation and a lower passive current density than stainless steel in NaOH solution, demonstrating a stronger ability to resist localized corrosion in alkaline corrosive environment.

For the potentiodynamic polarization curves in NaCl solution, the similar corrosion behaviors of coating and stainless steel can be found in Fig. 4(b) and Table 1. The corrosion potential of coating is about −0.472 V, which is higher than the stainless steel material as −0.846 V. The corrosion current density of coating is about

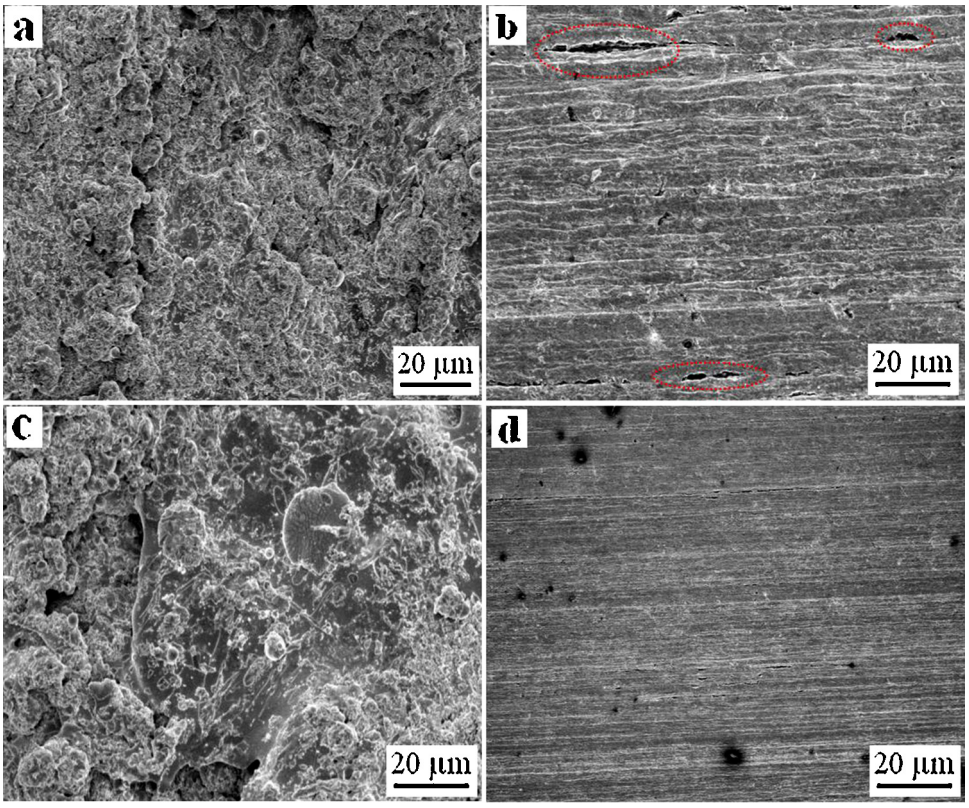

Fig. 5. SEM images of the surface after electrochemical test of (a) coating and (b) stainless steel in 2 mol/L NaOH solution, and (c) coating and (d) stainless steel in 3.5% NaCl solution.

5.623×10^{-6} A/cm^2, which is lower than the stainless steel material as 3.162×10^{-4} A/cm^2. The results from Fig. 4 (b) also demonstrate that coating exhibits higher corrosion resistance than 304 stainless steel material in simulated seawater solution.

Comparing the corrosion resistance of coatings in NaCl and NaOH solutions, it can be seen that the corrosion resistance of coating in NaCl solution is higher than the coating in NaOH solution. It is presumably attributed to the concentration of hydroxyl ion increased continuously during the polarization process, due to the chemical reaction on cathode: $O_2 + 2H_2O + 4e \rightarrow 4OH^-$. At the initial stage of the polarization process, the passive films can be formed in all solutions. As the concentration of hydroxyl ion increase, the unsteady passive films in the amorphous coating surface begin to dissolve.

Furthermore, the surface morphologies of coating and stainless steel in 2 mol/L NaOH solution after electrochemical test have been detected, as shown in Fig. 5(a) and (b). It can be seen that pitting corrosion and corrosion crack was found in surface, as indicated by circle in Fig. 5(b). Corrosive morphology can be seen, indicating that with high concentration NaOH solution, the amorphous coating is not effective to resist corrosion. Fig. 5(c) and (d) demonstrate the surface morphologies of coating and stainless steel after electrochemical measurement in 3.5% NaCl solution. It can be seen that the amorphous coating without any obvious pitting corrosion which is similar to their morphology before the testing showed in Fig. 2(a), indicating the high resistance to corrosion, as shown in Fig. 5(c). However, pitting corrosion was found in surface of stainless steel, as shown in Fig. 5(d).

The above results illustrate that the Fe-based metallic glass coatings deposited by AC-HVAF have much better corrosion than stainless steel, which is mainly dependent on their amorphous structure and chemical compositions. From the composition, both of amorphous coating and stainless steel have the Cr element, which is the element of self-passivation. For amorphous coating, the introduction of Cr element contributes to the formation of a strong passive film of hydrated chromium oxy-hydroxide. This process effectively inhibits the active dissolution of the amorphous phase and enhances the corrosion resistance as indicated by the results of previous work [23].

Besides, Mo element helps to promote the formation of passivation film and prevents the dissolution of Cr element during passivation, and B and C metalloid elements assist to increase the stability of the passivation films, both favoring to increase the corrosion resistance of the amorphous coatings[24]. It can be seen that stainless steel also has the self-passivation element of Cr and Ti. However, for stainless steel, when resistance to the solution containing of Cl^-, OH^- and F^-, the content of Cr element must be greater than 25% [25]. Meanwhile, from structure aspect, the Fe-based metallic glass coatings are almost free of grain boundaries, phase segregation and dislocation, and they can form homogeneous passivation films in corrosive environment, leaving no sensitive sites for pitting initiation.

4. Conclusions

Gas-atomized $Fe_{42.87}Cr_{15.98}Mo_{16.33}C_{15.94}B_{8.88}$ amorphous powders were deposited to form amorphous metallic coatings by HVAF thermal spraying. Microstructure studies have shown that the coatings deposited exhibit amorphous nature, dense layered structure and low porosity. The amorphous character of coating is due to the high glass forming ability and the high cooling rate of HVAF process. The corrosion behavior of the Fe-based amorphous coating was examined. The Fe-based amorphous coating had higher corrosion resistance in NaOH and NaCl solutions than stainless steel. However, the corrosion resistance of coating in NaOH is lower than the coating in NaCl solution. The

excellent corrosion resistance of Fe-based amorphous coating was attributed to the alloying elements and the homogeneous structure.

Acknowledgments

This work was supported by the National Natural Science Foundation of China (NSFC) under Grant No. 51205001, Key Project of Natural Science of Education Department of Anhui Province under Grant No. KJ2014A023, and Scientific Research Starting Foundation of Anhui Polytechnic University under Grant No. 2012YQQ006.

References

[1] Duwez P, Willens RH, Klement WJ. Continuous series of metastable solid solution in silver-copper alloys. Appl Phys Lett 1960;31:1137–40.
[2] Wang G, Fan HB, Huang YJ, Shen J, Chen ZH. A new TiCuHfSi bulk metallic glass with potential for biomedical applications. Mater Des 2014;54:251–5.
[3] Peker A, Johnson WL. A highly processable metallic glass $Zr_{41.2}Ti_{13.8}Cu_{12.5}Ni_{10.0}Be_{22.5}$. App Phys Lett 1993;63:2342–4.
[4] Shen J, Chen QJ, Sun JF, Fan HB, Wang G. Exceptionally high glass-forming ability of an FeCoCrMoCBY alloy. Appl Phys Lett 2005;86:151907.
[5] Xu DH, Lohwongwatana B, Duan G, Johnson WL, Garland C. Bulk metallic glass formation in binary Cu-Rich Alloy Series-$Cu_{10-x}Zr_x$ (x = 34, 36, 38.2, 40 at. %) and mechanical properties of bulk $Cu_{64}Zr_{36}$ glass. Acta Mater 2004;52:2621–4.
[6] Wang G, Miao DD, Xiao P, Huang ZJ, Chen ZH. Microstructure and corrosion behavior of Fe-based amorphous Alloy coatings by high velocity oxy fuel spraying. J Funct Mater 2014;11:19001–4.
[7] Huang YJ, Guo YZ, Fan HB, Shen J. Synthesis of Fe–Cr–Mo–C–B amorphous coating with high corrosion resistance. Mater Lett 2012;89:229–32.
[8] Cheng JB, Liang XB, Xu BS, Wu YX. Formation and properties of Fe-based amorphous/nanocrystalline alloy coating prepared by wire arc spraying process. J Non-Cryst Solids 2009;355:1673–8.
[9] Li CB, Chen WW, Jiang QS, Wang L, Luo D. Corrosion resistance of Ti-based metallic glass coating in concentrated nitric acid. Mater Chem Phys 2014;143:900–3.
[10] Li RF, Li ZG, Huang J, Zhu YY. Dilution effect on the formation of amorphous phase in the laser cladded Ni–Fe–B–Si–Nb coatings after laser remelting process. Appl Surf Sci 2012;258:7956–61.
[11] Zhu YY, Li ZG, Li RF. Microstructure and property of Fe–Co–B–Si–C–Nb amorphous composite coating fabricated by laser cladding process. Appl Surf Sci 2013;280:50–4.
[12] Ozdemir I, Ogawa K, Sato K. Iron boron based powders sprayed by high velocity spray processes. Surf Coat Tech 2014;240:373–9.
[13] Wang SL, Cheng JC, Yi SH, Ke LM. Corrosion resistance of Fe-based amorphous metallic matrix coating fabricated by HVOF thermal spraying. Trans Nonferrous Met Soc China 2014;24:146–51.
[14] Guo RQ, Zhang C, Chen Q, Yang Y, Li N, Liu LW. Study of structure and corrosion resistance of Fe-based amorphous coatings prepared by HVAF and HVOF. Corros Sci 2011;53:2351–6.
[15] Zhang C, Guo RQ, Yang Y, Wu Y. Influence of the size of spraying powders on the microstructure and corrosion resistance of Fe-based amorphous coating. Electrochim Acta 2011;56:6380–8.
[16] Li L, Kharas B, Zhang H, Sampath S. Suppression of crystallization during high velocity impact quenching of alumina droplets: observations and characterization. Mater Sci Eng A 2007;456:35–8.
[17] He J, Ice M, Lavernia E. Particle melting behavior during high-velocity oxygen fuel thermal spraying. J Therm Spray Technol 2001;10:83–93.
[18] Wang AP, Zhang T, Wang JQ. Formation and properties of Ni-Based amorphous metallic coating produced by HVAF thermal spraying. Mat Trans 2005;46:1010–3.
[19] Ye FX, Chen Y, Yu P, Luo Q, Qu SJ, Shen J. Structured analysis of iron-based amorphous alloy coating deposited by AC-HVAF spray. Acta Phys Sin 2014;63:078101–78106.
[20] Zhou Z, Wang L, Wang FC. Formation and corrosion behavior of Fe-based amorphous metallic coatings by HVOF thermal spraying. Surf Coat Tech 2009;204:563–70.
[21] Lin XH, Johnson WL. Formation of Ti–Zr–Cu–Ni bulk metallic glasses. J Appl Phys 1995;78:6514–9.
[22] Pang SJ, Zhang T, Asami K, Inoue A. Synthesis of Fe–Cr–Mo–C–B–P bulk metallic glasses with high corrosion resistance. Acta Mater 2002;50:489–97.
[23] Habazaki H, Kawashima A, Asami K, Hashimoto K. The effect of molybdenum on the corrosion behavior of amorphous Fe–Cr–Mo–P–C alloys in hydrochloric acid. Mater Sci Eng A 1991;134:1033–6.
[24] Tan MW, Akiyama E, Habazaki H, Kawashima A, Asami K, Hashimoto K. The role of chromium and molybdenum in passivation of amorphous Fe–Cr–Mo–P–C alloys in deaerated 1M HCl. Corros Sci 1996;38:2137–40.
[25] Wang L, Fan HB, Li J, Zheng W, Cao YS, Shen J. Corrosion behaviors of bulk amorphous $Fe_{41}Co_7Cr_{15}Mo_{14}C_{15}B_6Y_2$ alloy in HCl solution. Rare Met Mater Eng 2009;38:1992–6.